Transactions of the Materials Research Society of Japan 32[1] 193-197 (2007)

Higher-order Structure Analysis of Polyethylene Thin Films by *In-situ* Synchrotron Grazing-incidence Small-angle and Wide-angle X-ray Scattering Measurements

Sono Sasaki[1*], Hiroyasu Masunaga[1], Hiroo Tajiri[1], Hiroshi Okuda[2], Katsuaki Inoue[1], Atsushi Takahara[3], and Masaki Takata[1,4]

[1] *Japan Synchrotron Radiation Research Institute / SPring-8, Hyogo 679-5198, Japan;*
[2] *International Innovation Center, Kyoto University, Kyoto 606-8501 Japan;*
[3] *Institute for Materials Chemistry and Engineering, Kyushu University, Fukuoka 812-8581, Japan;*
[4] *The RIKEN Harima Institute / SPring-8, Hyogo 679-5198, Japan.*

The higher-order structures of high-density polyethylene (HDPE) thin films on Si wafers have been investigated on lamellar and molecular levels by synchrotron grazing-incidence small-angle and wide-angle X-ray scattering (GISWAXS: GISAXS and GIWAXS) measurements, respectively. Annealing effect on molecular orientation and lamellar stacking structure of the thin films was clarified by *in-situ* GISWAXS measurements at BL40B2 in SPring-8 for the thin films in a stepwise annealing process from 378 K to 393 K under vacuum. The thin films with a thickness of ca. 400 nm were prepared by a dip-coating method. The two-dimensional GISAXS patterns of the thin films suggested that crystalline lamellae were alternately stacked with amorphous in the parallel direction to the substrate surface and the long period increased from ca. 26 nm to ca. 36 nm during annealing. Their two-dimensional GIWAXS patterns measured at the same time indicated that HDPE chains formed the orthorhombic crystal and the chain axis in a crystalline lamella oriented relatively parallel to the film surface.

Key words: polyethylene thin film, synchrotron grazing-incidence small-angle and wide-angle X-ray scattering measurement, molecular orientation, lamellar stacking structure, annealing effect

1. INTRODUCTION

Physical properties of polymer materials strongly relate to their higher-order structures. In the case of crystalline polymer thin films, polymer chains are regularly packed to form crystals and crystalline lamellae are stacked with amorphous to form the so-called spherulite. Crystallographic properties of the films on molecular, lamellar and sherulitic scales directly influence their mechanical properties. For examples, the improvement in lamellar and molecular orientation enhances the strength and/or the modulus of elasticity of the films. Therefore, it is necessary to clarify the higher-order structure of polymer thin films to control their structural and physical properties and develop new functional polymeric materials.

Recently, grazing-incidence small-angle X-ray scattering (GISAXS) method has been improved as a suitable tool to evaluate meso-scale structures such as phase-separated structure of block copolymers and the size and dispersion of metal clusters grown on substrates. In-plane and out-of-plane structural information of the films can be obtained at the same time by two-dimensional (2D) GISAXS measurements. GISAXS analysis based on distorted wave Born approximation (DWBA) theory was applied for various multi-layer systems consisting of films and substrates. [1-11] On the other hand, grazing-incidence wide-angle X-ray diffraction (GIXD) method is a powerful tool for evaluating nano-scale structures of thin films. The authors reported crystal structure and crystallographic distortion for high-density polyethylene (HDPE) thin films investigated by in-plane GIXD measurements. [12-14] However, lamellar stacking structure and orientation in the thin films were under discussion.

The purpose of this study is to clarify the higher-order structure of HDPE thin films on the basis of a combination of GISAXS and GIXD methods. A synchrotron experimental method of grazing-incidence small-angle and wide-angle X-ray scattering (GISWAXS) was established for this study at BL40B2 in SPring-8. Annealing effect on the molecular orientation and lamellar aggregation structure was investigated by in-situ 2D GISWAXS measurements.

2. EXPERIMENTAL SECTION

2.1 Samples

A sample used in this study was additive free HDPE (Melt Index = 14) supplied from Mitsui Chemicals, Inc. as a typical example of crystalline polymers. Thin films with a thickness of ca. 400 nm were prepared onto the native oxide covered Si(110) surface of wafers with a 0.1 wt% *p*-xylene solution of HDPE by a dip-coating method. A Si wafer with a diameter of 1 inch was dipped into a *p*-xylene solution of HDPE heated at 373 K, and then the wafer was pulled up from the solution at a constant rate under N_2 atmosphere. The obtained films were isothermally crystallized at 373 K for 24 h from the melt under N_2 atmosphere. These melt-crystallized films were annealed at temperatures (*Ta*) of 378 K, 383 K, 388 K

or 393 K for 900s in a stepwise heating manner from 298 K to 453 K under vacuum.

2.2 Experiments

The surface morphology of HDPE thin films was observed by using an SPA400 (Seiko Instrument Industry, Co. Ltd., Japan) atomic force microscopy (AFM) in the contact operation mode at 298 K in air. The cantilever used in this study was triangle-shaped one with a quadrangular pyramidal Si_3N_4 cantilever tip (Olympus, Co. Ltd., Japan). The bending spring constants of the cantilevers were 0.02 Nm^{-1}. The long axis of the cantilevers was perpendicular to the scanning direction. The lamellar stacking distance was evaluated with the height profile in AFM images as shown in ref. 15.

In general, scattering from an organic thin film is relatively weak in intensity. Therefore, utilizing the high brilliance and highly parallel synchrotron X-rays as the incident beams is effective in detecting GISWAXS from HDPE thin films. In order to investigate molecular and meso-scale order structures of the films, synchrotron GISWAXS measurements were carried out with an imaging intensifier (II) + a charge coupled device (CCD) detector and imaging plate (IP) detectors at the BL40B2 in SPring-8 (Hyogo, Japan). Figs. 1a and 1b show experimental geometry of GISWAXS and a photograph of the *in-situ* GISWAXS experimental setup at BL40B2 in SPring-8, respectively. The components of the scattering vector, **q**, parallel and perpendicular to the sample surface were defined as $\mathbf{q}_y = (2\pi/\lambda)\sin(2\theta_f)\cos(\alpha_f)$ and $\mathbf{q}_z = (2\pi/\lambda)(\sin(\alpha_i) + \sin(\alpha_f))$, respectively, for reflected scattering. Here, λ is the wavelength of incident X-ray beams, α_i is the incident angle of X-ray beams, α_f is the exit angle, and $2\theta_f$ is the angle between the scattered beam and the plane of incidence. The

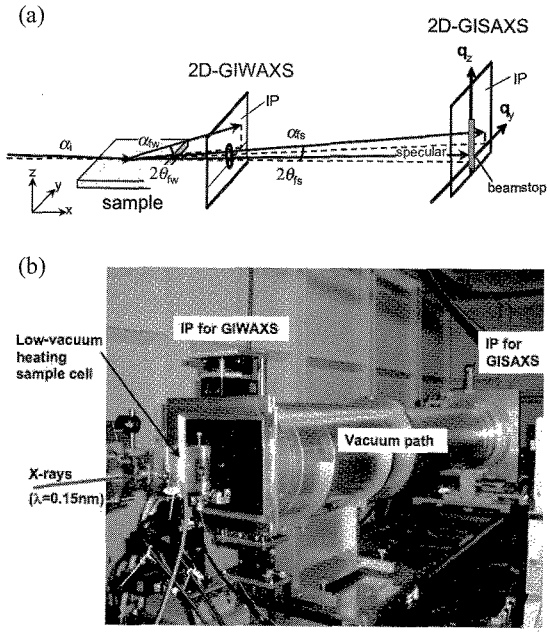

Fig. 1. Experimental geometry of GISWAXS (a) and a photograph of the *in-situ* GISWAXS experimental setup at BL40B2 in SPring-8 (b).

subscript s and w in Fig. 1 indicate GISAXS and grazing-incidence wide-angle X-ray scattering (GIWAXS) geometries, respectively. Nano-scale order structure such as chain-packing distance and chain orientation in the crystal region can be evaluated for the films by 2D GIWAXS measurements. On the other hand, meso-scale order structure such as lamellar stacking distance and lamellar orientation can be investigated for the films on the basis of 2D GISAXS data. The λ was 0.150 nm and the sample-to-detector distances were 107 mm for GIWAXS and 2196 mm for GISAXS. A 2m-length vacuum path was utilized between a sample cell and a detector for GISAXS measurements. The untransparent and semitransparent rectangular beamstops were connected each other and used for GISAXS measurements. Scattering patterns from the films were measured at the α_i of 0.13 and 0.20 deg., which were lower and higher than the critical angle of total external reflection at the surface of the PE film. The critical angles of the PE film, α_{cf}, and that of the Si wafer, α_{cs}, are 0.147 deg. and 0.215 deg., respectively, with λ = 0.150 nm. The surface-sensitive scattering pattern was obtained for the films at the α_i of 0.13 deg. The data collection time was 300 s per GIWAXS and GISAXS pattern with the IP detector.

In-situ simultaneous measurements of GISWAXS were carried out for the films at the *Ta* of 378 K, 383 K, 388 K and 393 K in a stepwise annealing process from 298 K to 453 K. The film on a Si wafer was placed on a heater stage of a low-vacuum sample cell and sample temperature was accurately monitored and controlled with an ultra-thin and wide K-type thermocouples and a program temperature controller. In order to reduce the intensity of background scattering, the window of the sample cell was covered with a 12.5 μm-thick Kapton film which was thinner than one utilized in our previous report. [16] At each *Ta*, GISWAXS from the film was measured for 300 s after annealing it for 600 s. The heating rate was ca. 10 deg./min and temperature fluctuation of the film at each *Ta* was ± 0.5 deg. Detectable **q**-ranges of GIWAXS and GISAXS in these experiments were ca. 4.3 nm^{-1} ~ 21 nm^{-1} and 0.05 nm^{-1} ~ 4.2 x 10^{-2} nm^{-1}, respectively.

3. RESULTS AND DISCUSSION

Figs. 2a, 2b, and 2c show AFM images of a HDPE thin film prepared by the dip-coating method, one crystallized isothermally at 373 K from the melt, and one annealed at 393 K for 24 h, respectively.

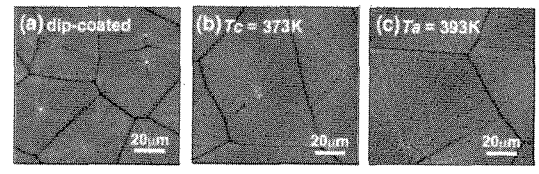

Fig. 2. AFM images of a HDPE thin film prepared by the dip-coating method (a), one crystallized isothermally at 373 K from the melt (b), and one annealed at 393 K for 24 h (c).

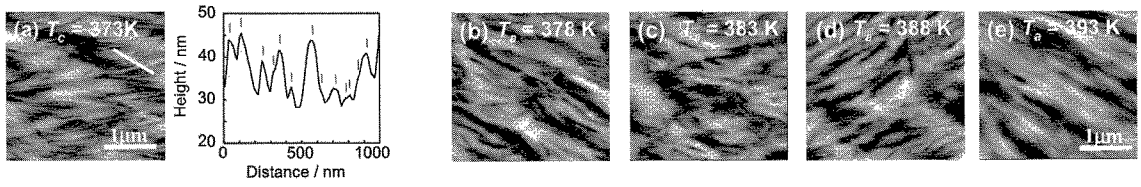

Fig. 3. High-resolution AFM images of the HDPE film isothermally crystallized at 373K (a), the annealed films at 378 K (b), 383 K (c), 388 K (d), and 393 K (e), and the height profile along a white line drawn in the image (a).

The brighter part in image contrast indicates the higher part in height. Each film was uniformly created on a Si wafer. As shown in Fig. 2a, two-dimensional spherulitic structure was formed in thin film by the dip-coating method. The center of the spherulite was locally higher in height than the other parts of the spherulite and the interface among spherulites was the lowest part. In Figs. 2b and 2c, spherulitic structure similar to that in Fig. 2a was observed. The size of spherulites generally depends on the number of the nuclei that is determined by the quality and quantity of impurities and the crystallization temperature. In the dip-coating treatment, temperature of the film during crystallization might decrease in N_2 atmosphere due to the latent heat of vaporization of the solvent. Therefore, spherulites in Fig. 2a looked smaller than those in Figs. 2b and 2c. It should be mentioned that sperulitic structure was also formed uniformly in the films annealed at 378 K, 383 K, and 388 K. Fig. 3a shows a high-resolution AFM image of the HDPE film crystallized isothermally at 373 K and the height profile along a white line drawn in the image. The peak-to-peak distance of the height profile indicates apparently the distance between adjacent lamellae at the surface of the film. Also, Figs. 3b, 3c, 3d, and 3e show high-resolution AFM images of the HDPE films annealed at 378 K, 383 K, 388 K, and 393 K for 24 h, respectively. The peak-to-peak distance was evaluated for the annealed films with their AFM height profiles in the same manner

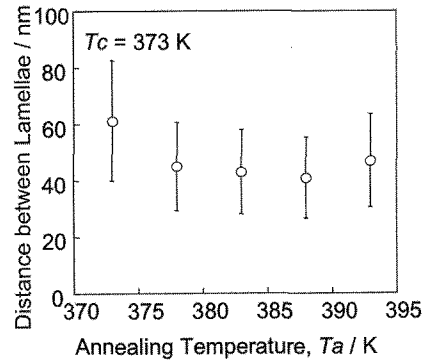

Fig. 4. Annealing temperature dependence of the distance between adjacent lamellae of the HDPE thin films evaluated with the height profiles of Figs. 3b ~ 3e. The distance between adjacent lamellae of the melt-crystallized film shown in Fig. 3a is also plotted as the initial state before annealing.

as the melt-isothermally crystallized film as shown in Fig. 3a. Fig. 4 shows annealing temperature dependence of the peak-to-peak distance between adjacent lamellae estimated in Figs. 3b ~ 3e and that of the melt-crystallized film shown in Fig. 3a as the initial state before annealing. The apparent lamellar

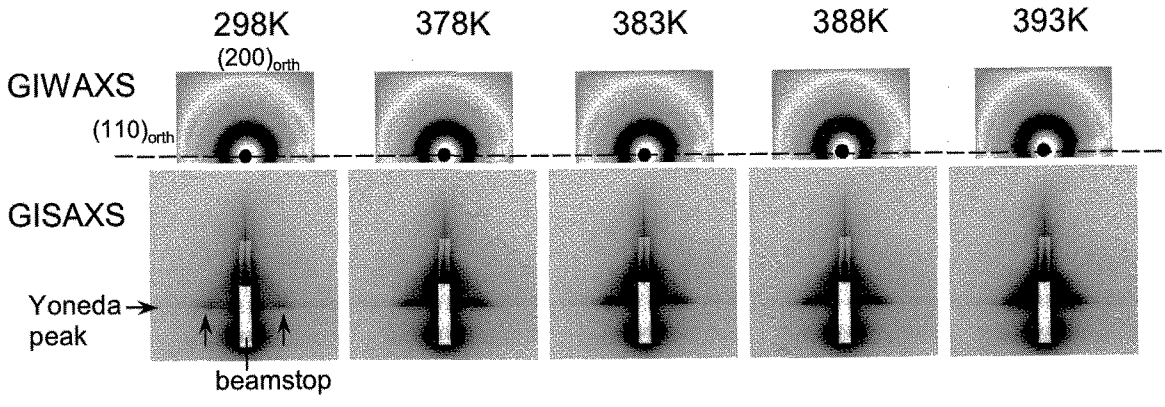

Fig. 5. *In-situ* GIWAXS and GISAXS patterns of a melt-crystallized HDPE film in the stepwise annealing process from 298 K to 393 K under vacuum. The α_i was 0.13 deg. The untransparent and semitransparent rectangular beamstops were connected each other and used for GISAXS measurements.

stacking distance at the film surface decreased at *Ta* = 378 K from ca. 60 nm to ca. 40 nm in average, and increased slightly to ca. 50 nm at *Ta* = 393 K. This implied that the stacking manner of main thick lamellae and the aggregation state of branched thinner lamellae might be changed at the film surface by annealing.

Fig. 5 shows *in-situ* GIWAXS and GISAXS patterns of a melt-crystallized HDPE film in the stepwise annealing process from 298 K to 393 K under vacuum. The α_i was 0.13 deg. As shown in the GIWAXS pattern of a melt-crystallized film at 298 K, the (110) and (200) reflections of the oriented orthorhombic crystal of HDPE were measured as broad peaks in the out-of-plane direction. The (200) reflection was measured at $\mathbf{q}_y$ = 0 deg. in the off-specular direction. Figs. 6a and 6b show intensity profiles plotted as a function of the azimuthal angle, φ, at the scattering angles of the peak tops of the orthorhombic (110) reflection (a) and (200) reflection (b) shown in the GIWAXS patterns of Fig. 5, respectively. The φ of 0 deg. and 180 deg. are on the in-plane line indicated with a broken line in Fig. 5 and the φ increases in the clockwise direction. These reflections were broad along $\mathbf{q}_z$, so that the peaks corresponding to the orthorhombic (110) reflection were also observed in Fig. 6b. As shown in Fig. 6a, the peaks corresponding to the orthorhombic (110) reflection were measured at φ = ca. 30 deg. ± 35 deg. and ca. 150 deg. ± 35 deg. Moreover, the peak corresponding to the orthorhombic (200) reflection was measured at φ = ca. 90 deg. ± 35 deg in Fig. 6b. These results indicated that the *a* axis of orthorhombic unit cell oriented relatively in the perpendicular direction to the film surface. In other words, the chain axis (the *c* axis) oriented relatively parallel to the film surface. The position and half-width of the peaks in Figs. 6a and 6b didn't change during annealing. The relative intensity of the orthorhombic (110) and (200) reflections increased with an increase in *Ta* as shown in GIWAXS patterns of Figs. 5a ~ 5e. This suggested that the degree of crystallinity of the thin films increased by annealing without change in crystallographic orientation.

On the other hand, the sharp scatterings near the Yoneda peak were measured in GISAXS patterns as shown with arrows in Fig. 5a. The Yoneda peak arises in the in-plane direction due to an interference effect of the incident and scattered wave. [17] This scattering increased in intensity with an increase in *Ta*, which suggested the increase in the degree of crystallinity and/or that in lamellar stacking regularity. The long period, the lamellar stacking distance, was estimated from the $\mathbf{q}_y$ of the peak in GISAXS patterns. Fig. 7a

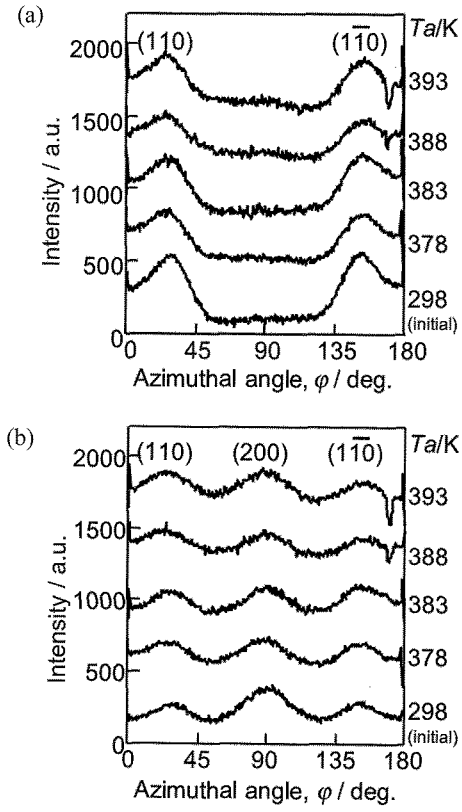

Fig. 6. Intensity profiles plotted as a function of the azimuthal angle, φ, at the scattering angles of the peak tops of the orthorhombic (110) reflection (a) and (200) reflection (b) shown in the GIWAXS patterns of Fig. 5.

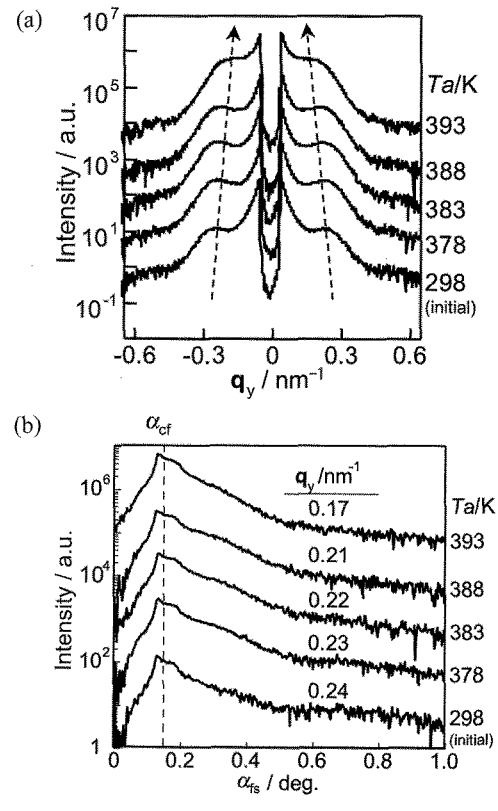

Fig 7. In-plane GISAXS profiles along the Yoneda peak (a) and out-of-plane GISAXS profiles at the $\mathbf{q}_y$ of the peaks in 7a (b). The α_{cf} is the critical angle of the HDPE films.

shows in-plane GISAXS profiles along the Yoneda peak in Fig. 5. The peak at 298 K before annealing was measured at $\mathbf{q}_y$ = ca. 0.24 nm^{-1} and shifted gradually to the lower $\mathbf{q}_y$ range with increasing *Ta*. The $\mathbf{q}_y$ of the peaks were ca. 0.23 nm^{-1} at 378 K, ca. 0.22 nm^{-1} at 383 K, ca. 0.21 nm^{-1} at 388 K, and ca. 0.17 nm^{-1} at 393 K. That is to say, the long period increased from ca. 26 nm to ca. 36 nm by annealing and a relatively large peak shift was measured at 393 K. Therefore, it should be mentioned that the *Ta* dependence of the long period was in good agreement with that of the apparent long period estimated from the peak-to-peak distance of adjacent lamellae in AFM height profiles as shown in Fig. 4. The apparent long period at the film surface estimated by AFM were larger than the long period measured by GISAXS. This might be due to difference in lamellar branching and stacking states between the film surface and film bulk. AFM images in Fig. 3 implied that several adjacent lamellae stuck one another to form an aggregate. Each lamella constructing the aggregate couldn't be clearly distinguished in AFM height profiles. Fig. 7b shows the out-of-plane GISAXS profiles at the $\mathbf{q}_y$ of the peaks in Fig. 7a. The α_{cf} in Fig. 7b is the critical angle of the HDPE films. The relative intensity of profile around the α_{fs} range of 0.2 deg. ~ 0.5 deg. changed slightly by annealing. This might relate to lamellar size and lamellar aggregation state in the out-of-plane direction. The 2D GISAXS patterns will be simulated with a stacked lamellar model and the four different wave vector transfers induced the refraction-reflection phenomena.

4. CONCLUSIONS

In this study, we have clarified annealing effect on the higher-order structure of crystalline polymer thin films by *in-situ* 2D-measurements of synchrotron GISWAXS at BL40B2 in SPring-8. The long period was successfully evaluated by synchrotron GISAXS measurements for the first time. The relationship between lamellar and molecular orientations and the lamellar stacking structure could be investigated for HDPE thin films with a thickness of 400 nm by GISWAXS measurements. *In-situ* GISAXS patterns suggested that crystalline lamellae were alternately stacked with amorphous in the parallel direction to the substrate surface and the long period was increased from ca. 26 nm to ca. 36 nm during annealing. This meso-scale phenomenon measured by GISAXS was in good agreement with that observed by AFM. *In-situ* GIWAXS patterns indicated that HDPE chains in the thin films formed the orthorhombic crystal and the chain axis in a crystalline lamella oriented relatively parallel to the film surface.

ACKNOWLEDGEMENTS

The authors would like to thank Dr. H. Yakabe for his great help in film preparation. The synchrotron radiation experiments were performed at the BL40B2 in the SPring-8 with the approval of the Japan Synchrotron Radiation Research Institute (JASRI) (Proposal No.: 2005B0655, 2006A1212, and 2006B1050).

REFERENCES

[1] P. Műller-Buschbaum, N. Hermsdorf, S.V. Roth, J. Wiedersich, S. Cunis, R. Gehrke, *Spectrochem. Acta Part B*, **59**, 1789-1797 (2004).
[2] S.V. Roth, P. Műller-Buschbaum, M. Burghammer, H. Walter, P. Panagiotou, A. Diethert, C. Riekel, *Spectrochem. Acta Part B*, **59**, 1765-1773 (2004).
[3] T. Xu, J. T. Goldbach, M. J. Minster, S. Kim, A. Gibaud, O. Gang, B. Ocko, K. W. Guarini, C. T. Black, C. J. Hawker, T. P. Russell, *Macromolecules*, **37**, 2972-2977 (2004).
[4] B. Lee, W. Oh, J. Yoon, Y. Hwang, J. Kim, B. G. Landes, J. P. Quintana, M. Ree, *Macromolecules*, **38**, 8991-8995 (2005).
[5] B. Lee, W. Oh, Y. Hwang, Y. -H. Park, J. Yoon, K. S. Jin, K. Heo, J. Kim, K. -W Kim, M. Ree, *Adv. Mater.*, **17**, 696-701 (2005).
[6] B. Lee, I. Park, J. Yoon, S. Park, J. Kim, J. Kim, K. -W. Kim, T. Chang, M. Ree, *Macromolecules*, **38**, 4311-4323 (2005).
[7] B. Lee, J. Yoon, W. Oh, Y. Hwang, K. -S. Heo, K. -S. Jin, J. Kim, K. -W. Kim, M. Ree, *Macromolecules*, **38**, 3395-3405 (2005).
[8] B. Lee, Y. -H. Park, Y.-T. Hwang, W. Oh, J. Yoon, M. Ree, *Nature Mater.*, **4**, 147-150 (2005).
[9] I. Park, B. Lee, J. Ryu, K. Im, J. Yoon, M. Ree, T. Chang, *Macromolecules*, **38**, 10532-10536 (2005).
[10] C. Tang, A. Tracz, M. Kruk, R. Zhang, D. -M. Smilgies, K. Matyjaszewski, T. Kowalewski, *J. Am. Chem. Soc.*, **127**, 6918-6919 (2005).
[11] B. Chung, M. Choi, M. Ree, J. C. Jung, W. C. Zin, T. Chang, *Macromolecules*, **39**, 684-689 (2006).
[12] H. Yakabe, S. Sasaki, O. Sakata, A. Takahara, T. Kajiyama, *Macromolecules*, **36**(16), 5905-5907 (2003).
[13] H. Yakabe, S. Sasaki, O. Sakata, A. Takahara, T. Kajiyama, *Trans. Mater. Res. Soc. Jpn*, **29** (1), 251-254 (2004).
[14] H. Yakabe, K. Tanaka, T. Nagamura, S. Sasaki, O. Sakata, A. Takahara, T. Kajiyama, *Polym. Bull.*, **53**, 213-222 (2005).
[15] S. Sasaki, Y. Sakaki, A. Takahara, T. Kajiyama, *Polymer*, **43**, 3441-3446 (2002).
[16] S. Sasaki, H. Masunaga, H.Tajiri, K. Inoue, H. Okuda, H. Noma, K. Honda, A. Takahara, M. Takata, *J. Appl. Crystallog.*, **40**, *to be published* (2007).
[17] Y. Yoneda, *Phys. Rev.*, **131**, 2010-2013 (1963).

(Received December 9, 2006;Accepted March 1, 2007)